A LATERAL-EFFECT PHOTODIODE SCANNING SENSOR FOR AUTONOMOUS VEHICLE MANOEUVRES

N.E. PEARS and P.J. PROBERT

Department of Engineering Science, University of Oxford
19 Parks Road, Oxford, 0X1 3PJ, England.

Abstract A large field of view laser scanning sensor, based on the lateral-effect photodiode, and designed for close range mobile robot manoeuvres, is described. Laser modulation and synchronous detection are used to approach the theoretical white noise limit of sensor performance. Noise in the system, which determines ranging accuracy, is determined from logarithmic plots of signal strength and image resolution against range. The results suggest that sensor accuracy is around 82% above the theoretical performance limit. Finally, some typical scans are presented.

Key Words. Robots; sensors; signal detection; signal processing; guidance systems

1. INTRODUCTION

The development of good sensors is a central area of robotics research. For close range mobile robot manoeuvres, such as obstacle avoidance and docking, an active optical means of acquiring range data has been chosen. Such methods are generally more robust than sonar methods, are computationally simpler and cheaper than passive vision methods, and can acquire range data at a higher bandwidth than both. Our sensor is active, both in the sense that it uses structured light and in the sense that it can rotate its whole body in a horizontal plane and dynamically modify its angular scan pattern within a 40 degree range.

To obtain performance near to the theoretical limit, which is determined from the detector and preamplifier white noise density over the measurement bandwidth, a synchronous detection method has been employed. Furthermore, in order to provide simultaneously a wide field of view and a large depth of field, a synchronised scanning triangulation geometry has been implemented.

In the next section, the choice of optical source and image sensor and the electronic and geometric design of the sensor are described. Section 3 presents a noise analysis and the final section before the conclusions presents sensor accuracy results and compares them with theoretical prediction. Also in this section, some typical scans are presented; a first approach to processing this scan data is given in Pears and Probert (1993).

2. SENSOR DESIGN

2.1 *Image Position Sensor*

For an image position sensor, the LEP rather than the more commonly used CCD has been chosen. The LEP is often cheaper and simpler to use than a CCD and can offer a greatly improved image position resolution at shorter ranges. The range at which a CCD system begins to outperform an LEP system depends on many optical, geometric, and electrical parameters. Our system requires ranges over 1m before a 1024 pixel CCD (one-pixel resolution) becomes more accurate than a simple LEP.

2.2 *Optical Source*

The optical source employed is a 670nm laser diode which is modulated at 10kHz and projects an average power of 0.9mW into the scene. This power complies with the class II limit (1mW) for visible lasers. The laser is attractive since its fine collimation brings the advantages of specific localised probing of the environment, compact scanning optics, and a small image size. In addition, its spectral purity allows the use of very narrow band optical filters to reject ambient light. The great problem of a laser, when projected into an open environment, is the eye safety problem, which sets an upper limit on the power output.

2.3 *Electronic Design*

Careful circuit design for low noise performance is required for the efficient use of an LEP. The 10kHz modulation on the laser diode allows the use of synchronous detection in the receiver to maximise signal to noise ratio and eliminate dc offsets. The key elements of the design are described in the following subsections.

Transimpedance preamplifier. This is designed with three specifications in mind: low noise density (required for good image position resolution), very high gain (required to detect signals of a few nanoamps) and a wide bandwidth (required to include the first few harmonics of the 10kHz modulation).

Synchronous detector. This is required to centre the signal content around the harmonics of the modulation, thus avoiding the effects of ambient light, dc offsets and drifts in the preamplification stages, and flicker ($\frac{1}{f}$) noise. This allows the sensor to approach the theoretical limit of performance as defined by the white noise density over the measurement bandwidth.

Low pass filter. A low pass filter at the end of the signal detection chain defines the measurement bandwidth of the system. This must be set considerably below the modulation frequency, at a level which is an appropriate compromise between signal to noise ratio and speed of response. Our filter is a fourth order filter with gain 1.9 and 3db cut off at 1kHz. Since this stage dominates the dynamic response of the system, a Bessel response was chosen to avoid any ringing at edges in the range scan.

2.4 *Geometric design*

A technique called synchronised scanning is often employed in multi-dimensional optical ranging in order to maintain a uniform triangulation geometry as the sensor scans over the scene. A synchronised scheme has been adopted, as suggested by Rioux (1984), in which the scan direction is parallel to the detector field of view. In this geometry (see fig. 1), the scanned beam is tracked by an imaging mirror so that the angular separation between the projection axis and the optical axis of the lens remains constant.

If it is assumed that the range of the object is large compared with the focal length of the collecting lens, then the focal plane is at a distance f from the principal point of the lens, and simple geometrical analysis yields

$$z = \frac{fd}{p}cos^2\theta + \frac{d}{2}sin2\theta \qquad (1)$$

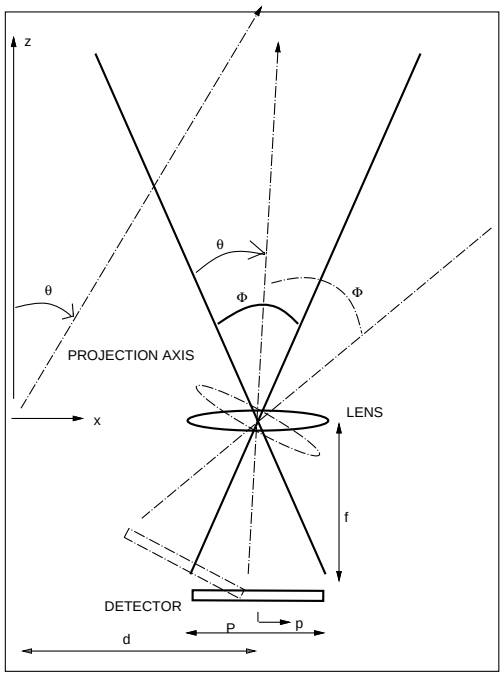

Fig 1. Schematic synchronised scanning geometry

$$x = ztan\theta \qquad (2)$$

In the limit, the ratio of image resolution to range resolution is defined as the triangulation gain (G_p) and, from (1), is given by

$$\frac{\partial p}{\partial z} = G_p = \frac{fdcos^2\theta}{z^2} \qquad (3)$$

Thus, for a given image resolution, ranging accuracy is proportional to source/detector separation and focal length, decreases with the inverse square of range, and decreases, moving away from the centre of a scan, by the square of the cosine. The cost of increasing accuracy with a larger baseline is a bulkier sensor and greater susceptibility to the missing parts problem. The cost of increasing accuracy by increasing focal length is a proportional reduction in the depth of field. To provide a depth of field of 0.4m to 2.5m, whilst observing these tradeoffs, a baseline $d = 9.5cm$, a focal length $f = 5cm$, and a detector length $P = 1cm$ have been employed.

Note also that, in addition to finite image resolution, there is an effect on ranging accuracy developed by the error in measurement of the projection angle. Partial differentiation of (1) gives

$$\frac{\partial \theta}{\partial z} = G_\theta = \frac{1}{dcos2\theta - 2ztan\theta} \qquad (4)$$

A synchronised scanning head was designed. Fig. 2 shows a plan view of the sensor, which is 21cm wide, 16cm deep, and 4.2cm high. Referring

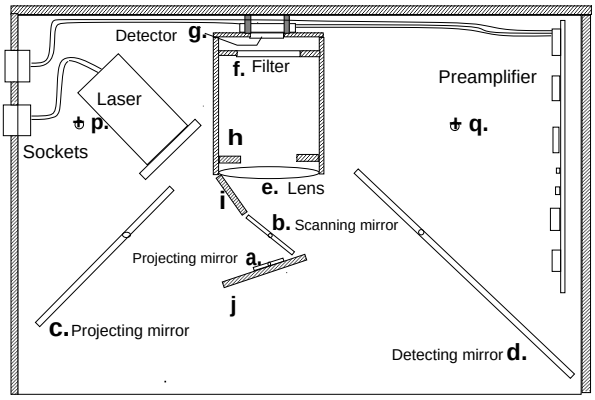

Fig 2. The obstacle avoidance sensor

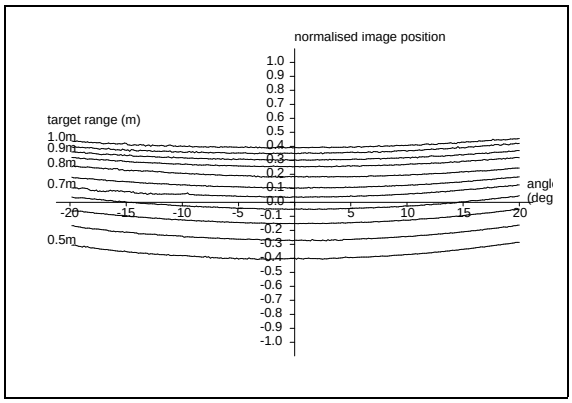

Fig 3. Calibration curves: image position against scan angle

to the figure, a collimated and modulated laser beam is projected onto a small mirror (a), which deflects the beam onto the front face of the scanning mirror (b). The use of this small mirror prevents the laser body from blocking the sensor aperture. The scanned beam is then projected into the scene by a larger mirror (c), which can be pivoted to set the direction of the projection angle when the scanning mirror is at rest in its zero position. With this arrangement, the laser is scanned over twice the angle over which the scanning mirror deflects, and the centre of scanning is at the virtual image point p in the sensor. Laser light, scattered by objects in the scene, is collected by the large adjustable detection mirror (d) and is deflected onto the rear of the scanning mirror. Light leaving the scanning mirror is focussed by the lens (e) and passes through an optical filter (f), matched to the laser wavelength, before forming an image of the projected spot on the lateral-effect photodiode (g). To minimise noise, the detector signals are amplified inside the camera head before being passed to the synchronous detector in the sensor interface rack.

With the geometry described above, the lens is effectively scanned around virtual image point q in the sensor on an arc with radius equal to the separation between the scanning mirror and the lens. In our design, this separation is kept as small as possible to minimise variations in triangulation baseline over the scanning range. The dimensions and positioning of the detection mirror (d) are critical and ensure that the full sensor aperture (the full surface of the scanning mirror) is accessible over all combinations of scan angle and target range.

The sensor is designed with as large an aperture as possible that is consistent with our scanning requirements because of the LEP's dependence on a good signal to noise ratio. Most of the aperture derives from the depth of the scanning mirror (4cm) rather than its width (2.2cm) in order to limit rotational inertia. Direct optical paths, in which laser light is focussed directly from the scene onto the LEP, have been prevented with the use of a 'cats-eye' aperture stop (h) behind the lens and shielding plates (i) and (j).

Fig. 3 shows the recorded image position as the sensor scanned across a planar target at ranges of 0.5 to 1.0m. Since the lens is scanned in synchronism with the laser, there is only a small variation in image position over the scanning range. The fall in triangulation gain with target range is shown by the decreasing separation of the image position curves.

The final specifications of the sensor are: field of view (scan range) 40 degrees, depth of field (z range) 0.4m to 2.5m, samples per horizontal scan 256, scan frequency 10Hz, sample frequency 2.56kHz, projected laser power 0.9mW at 670nm (class II), detector bandwidth 1kHz (set by fourth order Bessel filter).

3. NOISE ANALYSIS

A comparison of the actual performance of the sensor and the performance predicted from the specifications of the LEP, preamplification electronics and sensor geometry is essential to determine how close the sensor is to the physical limits of ranging accuracy. In the following analysis, only the effect of image position resolution on ranging resolution is considered. However, in a scanning sensor, errors in scan angle measurement will also contribute to ranging error. The specifications of our scanner quote a mirror angle repeatability of 0.1mrad which makes that the effect of scan angle resolution on accuracy negligible.

3.1 *Experimental Conditions*

The sensor was set up with the laser pointing along the z-axis and image position, p, was cal-

ibrated against range, z. A target, consisting of an off-white cardboard box was set up at ranges between 0.75m and 2.5m in steps of 0.25m. At each range, 1000 measurements of signal current, I_s, and normalised image position, p, were made. For each image position measurement, range, z, was interpolated from the calibration look up table.

3.2 *System Noise Estimation*

Using logarithmic plots of averaged signal current against range and image resolution (the standard deviation of image position) against range, the effective noise density in the system can be calculated.

If it is assumed that the projected spot is small enough and distant enough to be treated as a point source and that purely lambertian scattering occurs in the scene, then the total signal current I_s at range z, for laser power P_l, can be approximated by

$$I_s = \frac{S}{z^2} \tag{5}$$

The signal current constant, S, is given by (Pears and Probert, 1992)

$$S = \frac{\rho A cos\theta_d T_1 T_2 R_\phi P_l}{2\pi} \tag{6}$$

where ρ is scene reflectivity, A is aperture (m^2), θ_d is the orientation of the aperture with respect to the target surface, T_1 is the reflectivity of the projection optics, T_2 is the reflectivity of the detection optics, R_ϕ is the responsivity of the LEP (A/W) and P_l is the power projected by the laser (W).

Rather than measuring or estimating these individual parameters, in which case the errors in each value would contribute to the error in the estimation of the sensor performance, the composite parameter, S, can be measured directly from a logarithmic plot of signal current against range. This plot is given in fig. 4 where the crosses represent the actual measurements and the solid line is a least squares fit. The intersection of the regression at the y-axis gives

$$S = 2.59 \times 10^{-8} Am^2 \tag{7}$$

Now, image resolution for an LEP is

$$\Delta p = \frac{P}{2\frac{I_s}{I_n}} \tag{8}$$

where P is the detector length and $\frac{I_s}{I_n}$ is the signal current to noise current ratio of the detection. Since image position measurements are normalised to lie in the region $\{-1 \leq p \leq 1\}$, then

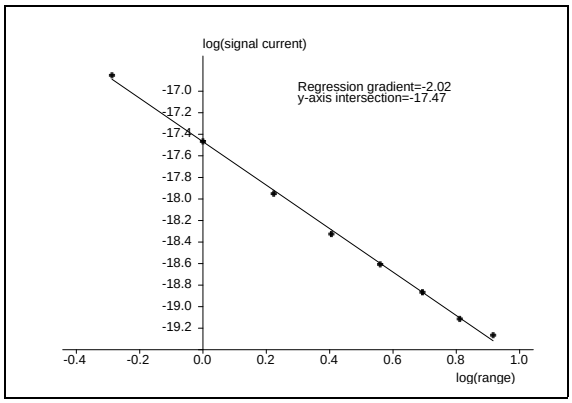

Fig 4. Logarithmic plot of signal current against range

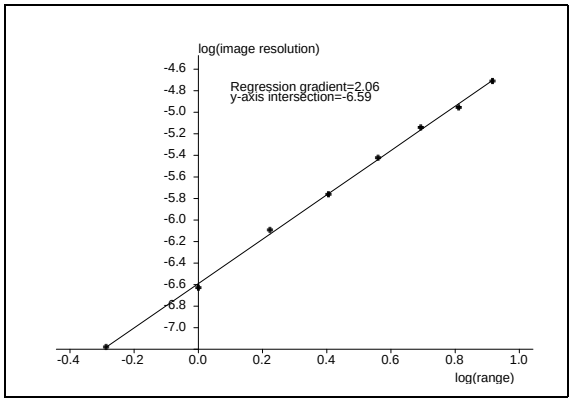

Fig 5. Logarithmic plot of image resolution against range

$$\Delta p_{norm} = \frac{I_n}{I_s} = \frac{I_n z^2}{S} \tag{9}$$

where I_n is the total noise current over the measurement bandwidth. Thus a logarithmic plot of image resolution against range, given in fig. 5, gives the constant $\frac{I_n}{S}$ and thus the noise current I_n

$$I_n = 36.5pA \tag{10}$$

In these tests, the measurement bandwidth was set by a fourth order low pass Bessel filter with cut off at 1kHz. Thus the approximate current noise density, assuming an ideal filter response, is

$$i_n = 1.15pAH z^{-\frac{1}{2}} \tag{11}$$

3.3 *Theoretical Noise Calculation*

In calculating the theoretical noise density, it is assumed that shot noise due to the signal current, and shot noise due to any current generated by ambient light passing through the optical filter, are negligible.

The total detector noise density is the rms summation of shot noise from the dark current and thermal noise. For the LEP, dark current $I_d = 100nA$, $R_s = 50k\Omega$, and assuming $T = 298K$:

$$i_{nd} = \sqrt{2eI_d + \frac{4kT}{R_s}} = 0.6pAHz^{-\frac{1}{2}} \qquad (12)$$

Preamplifier noise, including feedback resistor noise is given as:

$$i_{na} = \sqrt{i_{n_a}^2 + \frac{e_{n_a}^2}{R_s} + \frac{4kT}{R_f}} = 0.2pAHz^{-\frac{1}{2}} \quad (13)$$

Calculating the rms of (12) and (13) gives the total current noise density (I_n) for the detector-preamplifier combination as $0.632pAHz^{-\frac{1}{2}}$. The noise density calculated from measurements ($1.15pAHz^{-\frac{1}{2}}$) is only 82% above this value which shows that the use of synchronous detection has allowed us to get close to the theoretical performance limit of the sensor.

4. SENSOR ACCURACY

4.1 *Measured Accuracy*

Fig. 6 shows a histogram of range measurements when a target was placed at 1m from the sensor, and 1000 readings were taken. In this figure, the crosses show the frequency with which a measurement fell within a particular range interval. The solid line shows the equivalent Gaussian, generated using mean and standard deviation of the batch of 1000 measurements. From fig. 6 it is evident that, in any processing of the raw sensor data, the assumption of of a Gaussian form is reasonable. Standard deviations for all target ranges, and their values as a percentage of the target range, are shown in table 1.

Table 1. Ranging accuracy

range(m)	SD (cm)	% accuracy
0.75	0.05	0.067
1.0	0.148	0.148
1.25	0.463	0.37
1.5	0.798	0.532
1.75	1.568	1.1
2.0	2.547	1.27
2.25	3.713	1.65
2.5	7.662	3.06

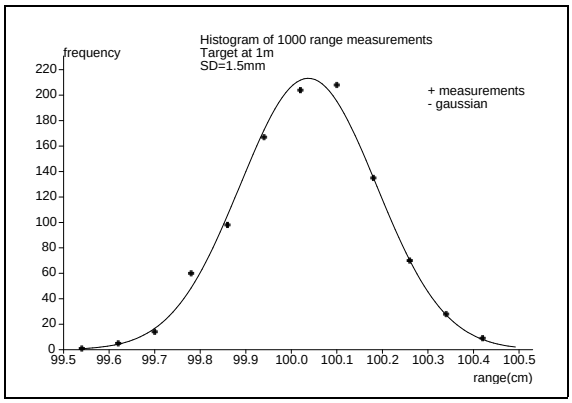

Fig 6. The distribution of range measurements at 1m

4.2 *Predicted Accuracy*

In order to calculate range resolution from image position resolution the triangulation gain constant, fd, must be estimated. Combining (9) and (3) for $cos\theta = 1$ gives

$$\Delta z = Tz^4 \qquad (14)$$

where

$$T = \frac{PI_n}{2fdS} \qquad (15)$$

Thus, a logarithmic plot of Δz against z will give the constant T and, since I_n and S are known from previous logarithmic plots, fd can be obtained. The intersection of the regression line with the y-axis in such a plot gives $fd = 0.0044m$.

Range resolution against range can now be plotted for the measured noise density ($1.15\ pAHz^{-\frac{1}{2}}$) and the theoretical noise density ($0.632\ pAHz^{-\frac{1}{2}}$) using equations (14) and (15). These two plots, and the points at which ranging accuracy was measured (from table 1), are shown in fig. 7.

When scanning, ranging accuracy will be poorer at the edges of the scan than at the centre since, from (3), triangulation gain drops with $cos^2\theta$ and, to compound this, signal strength will be reduced because of the apparent reduction in aperture with $cos\theta$. The total effect is to reduce ranging accuracy at the edges of a scan to around 83% of its value at the centre. The results given in the following section show that this variation of ranging accuracy with scan angle is small compared to the variation of ranging accuracy with range.

4.3 *Scanning Performance*

Finally, raw sensor scans are presented to illustrate the high performance in detecting edges

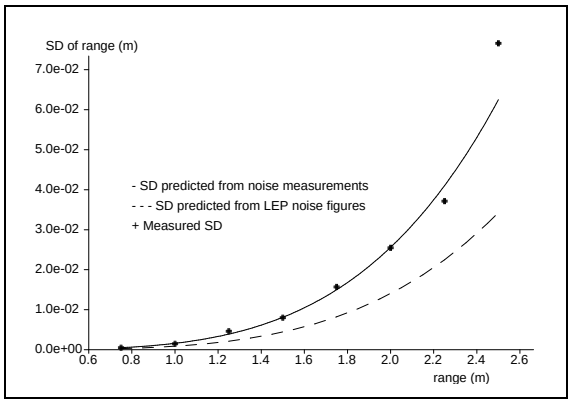

Fig 7. Plot of predicted and actual SD of range against range

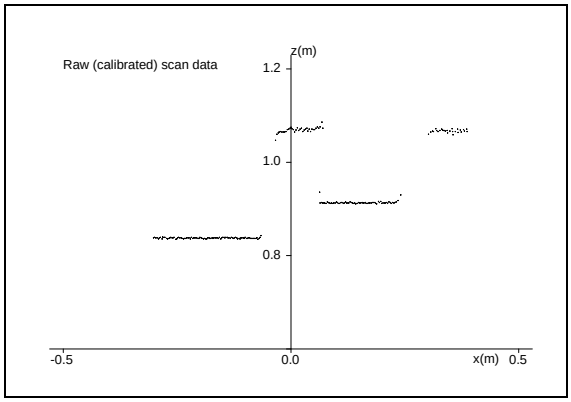

Fig 8. Scene with boxes

and curves. The first plot fig. 8, shows the excellent response over abrupt edges. The second plot, fig. 9a, shows the scan over a cylindrical object. It has been noted that signal amplitude data may be useful for localisation of certain types of feature. Fig. 9b illustrates that, in the case of a cylindrical object, a distinct peak is found at the centre of the feature.

5. CONCLUSIONS

A wide field of view optical range sensor designed for close range mobile robot manoeuvres has been described. Measurements have shown that ranging is accurate to 0.15% at 1m, 1.3% at 2m and 3% at 2.5m for a measurement bandwidth of 1kHz, which is suitable for real-time planning, and an average projected power of 0.9mW which is eye-safe. These figures compare well with other rangefinders available at comparable cost. In addition, the application range of LEPs has been extended, since they are normally used over a restricted range with none eye-safe lasers.

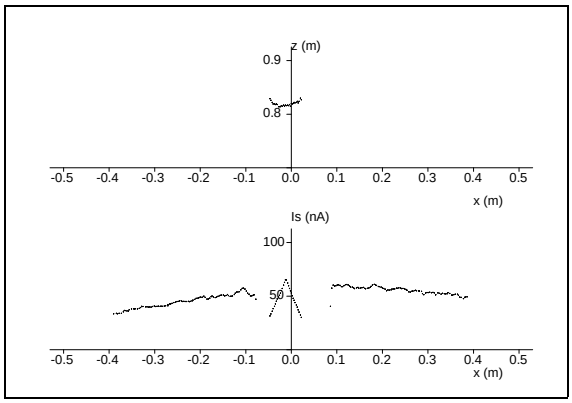

Fig 9. Cylinder

6. REFERENCES

Pears, N.E., and P.J. Probert (1992). Active triangulation rangefinder design for mobile robots. In: *Proc. IEEE/RSJ Int. Conf. on Intelligent Robots and Systems*, pp 2047-2052.

Pears, N.E., and P.J. Probert (1993). An optical range sensor for mobile robot guidance. To be published in: *Proc. IEEE Int. Conf. on Robotics and Automation.*

Rioux, M. (1984). Laser rangefinder based on synchronised scanners. In: *Applied Optics*, **23**(21), pp 3837-3834.